Modern Pathology (2021) 34:1710–1718
https://doi.org/10.1038/s41379-021-00830-w

ARTICLE

Superficial *ALK*-rearranged myxoid spindle cell neoplasm: a cutaneous soft tissue tumor with distinctive morphology and immunophenotypic profile

Josephine K. Dermawan[1] · Elizabeth M. Azzato[1] · John R. Goldblum[1] · Brian P. Rubin[1] · Steven D. Billings[1] · Jennifer S. Ko[1]

Received: 8 March 2021 / Revised: 3 May 2021 / Accepted: 5 May 2021 / Published online: 4 June 2021

Abstract

Gene rearrangements involving the anaplastic lymphoma kinase (ALK) receptor tyrosine kinase gene have been identified in various neoplasms, including inflammatory myofibroblastic tumor and epithelioid fibrous histiocytoma. We present an *ALK*-rearranged cutaneous soft tissue tumor with unique morphologic and immunophenotypic features that are not shared by other entities with *ALK* rearrangements. The six cases involved two females and four males, aged 18–84 (mean 51) years old. Three tumors were on the back and three on the lower extremities (thigh, knee, shin); ranging from 0.5 to 5.6 (mean 2.1) cm. Four were confined to the dermis; two involved the subcutis. All six cases were characterized by the presence of spindled to ovoid cells arranged in concentric whorls and cords against a myxoid to myxohyaline stroma and relatively cellular aggregates of plump ovoid to epithelioid cells. Four cases showed distinct hyalinized blood vessels. Both cases that involved the subcutis showed peripheral lipofibromatosis-like areas. Tumor-infiltrating lymphocytes were absent to moderate. Severe cytologic atypia or conspicuous mitotic activity was not identified. Immunohistochemically, all tumors diffusely expressed ALK (D5F3) and CD34. All but one tumor was diffusely positive for S100 protein. All tumors were negative for EMA, AE1/AE3, SMA, and SOX10. Next-generation sequencing revealed *ALK* fusions with *FLNA* (3 cases), *MYH10* (2 cases), and *HMBOX1* (1 case) as the partner genes. In all six cases, the breakpoints involved exon 20 of *ALK*, which preserves the receptor tyrosine kinase domains of ALK in the fusion product. Of the four cases with limited follow-up information (2–18 months), none recurred. In conclusion, we report an *ALK*-rearranged cutaneous soft tissue tumor characterized by the presence of myxoid spindle cell whorls and cords, and co-expression of ALK, CD34, and frequently S100 protein, we term "superficial *ALK*-rearranged myxoid spindle cell neoplasm".

Introduction

Encoded by a genomic locus at chromosomal band 2p23, the anaplastic lymphoma kinase (ALK) receptor tyrosine kinase (RTK) is a member of the insulin receptor kinase superfamily gene that has been implicated in both normal development and oncogenesis [1–3]. Similar to other RTKs, ALK possesses an extracellular ligand-binding domain, a transmembrane-spanning domain, and a cytoplasmic kinase catalytic domain [1–3]. *ALK* gene fusions have been identified in numerous neoplastic processes, including 2–7% of non-small cell lung cancers [4], ALK-positive anaplastic large cell lymphomas [5], inflammatory myofibroblastic tumors [6], epithelioid fibrous histiocytomas [7, 8], and atypical spitzoid neoplasms [9].

An emerging class of spindle cell tumors defined by S100 protein and CD34 co-expression and characterized by recurrent tyrosine kinase fusions involving *NTRK1/2/3* [10–13], *BRAF* [10, 14], *RAF1* [10], and *RET* [15, 16] has been reported over the past few years. Recently, a follow-up study of 73 soft tissue tumors with kinase fusions identified two cases with *ALK* gene fusions [17]. Additional single case reports of soft tissue and bone tumors with *ALK*-rearrangement and S100 and CD34 co-expression have been reported [18–20]. We present the

These authors contributed equally: Steven D. Billings, Jennifer S. Ko

✉ Jennifer S. Ko
koj2@ccf.org

[1] Robert J. Tomsich Pathology & Laboratory Medicine Institute, Cleveland Clinic, Cleveland, OH, USA

first case series of an *ALK*-rearranged cutaneous soft tissue tumor with unique histopathologic and immunophenotypic features that are not shared by other entities with *ALK* rearrangements.

Materials and methods

Patient cohort and data collection

After obtaining approval from the Institutional Review Board (IRB), cases sequenced by our solid tumor next-generation sequencing (NGS) fusion panel were reviewed. Slides for cutaneous tumor cases containing *ALK* gene fusions were retrieved and the histomorphology was reviewed. We collected the following clinical parameters: patient age, sex, tumor size, location, and follow-up information when available, and the following pathologic parameters: cytomorphologic and histologic features, mitotic rate, and presence of atypia. Available previously performed immunohistochemical stains were reviewed.

Immunohistochemical staining

Paraffin blocks or unstained slides, when available, were retrieved from the archives of the Department of Pathology at Cleveland Clinic. An immunohistochemical study was carried out using the Ventana Benchmark Ultra automated immunostainer [Ventana Medical Systems (VMS), Tucson, AZ]. Localization of the antigen–antibody complex was achieved using the VMS OptiView DAB detection kit. For ALK (clone D5F3), slides were stained by incubation with a rabbit monoclonal antibody (Cell Signaling Technology cat# 3633 S, Danvers, MA) at 1:100 dilution for 32 min at 37 °C. For CD34, slides were stained by incubation with a prediluted mouse monoclonal antibody (Cell Marque cat# 134M-18, Rocklin, CA) for 16 min at 37 °C. For S100, slides were stained by incubation with a prediluted rabbit polyclonal antibody (Agilent [Dako] cat# IR50461-2, Santa Clara, CA) for 32 min with no heat. For epithelial membrane antigen (EMA), slides were stained by incubation with a mouse monoclonal antibody (Agilent [Dako] cat# M061301-2, Santa Clara, CA) at 1:50 dilution for 16 min at 37 °C. For pancytokeratin AE1/AE3, slides were stained by incubation with a mouse monoclonal antibody (Millipore cat# MAB3412, Burlington, MA) at 1:200 dilution for 12 min at 37 °C. For smooth muscle actin (SMA), slides were stained by incubation with a mouse monoclonal antibody (Agilent [Dako] cat# M085101-2, Santa Clara, CA) at 1:50 dilution for 12 min at 37 °C. For SRY-related high-mobility group HMG box gene 10 (SOX10), slides were stained by incubation with a predilute mouse monoclonal antibody (Biocare Medical cat# AVI3099G, Pacheco, CA) for 32 min at 37 °C. All immunohistochemical signals were then detected using the Ventana OptiView DAB Detection Kit (Ventana).

For immunohistochemistry, negative is defined as 0%, focally positive 1–50%, and diffusely positive >50%.

Next-generation sequencing

Details of the solid tumor NGS fusion panel were previously published [21]. In brief, 5–10 unstained slides and 1 hematoxylin and eosin-stained slide from neutral buffered formalin-fixed, paraffin-embedded tissue sectioned at 4 µm were obtained from each specimen. Complementary DNA libraries were made using anchored multiplex polymerase chain reaction (Archer FusionPlex standard protocol and reagents, Archer DX, Inc., Boulder, CO) and custom-designed gene-specific primer pools, targeting the 58 genes included in this panel that is involved in BST tumors. (Note: this panel was updated from the previous versions in the cited paper to include additional targets.) Sequencing was performed on the MiSeq instrument (Illumina, San Diego, CA) with 151 × 2 cycle pair-end reads to a depth of >500,000 total reads. Results from Archer analysis software (Version 6.0.3.2) and an in-house informatics pipeline were used for read alignment (genome build hg19/GRCh37), fusion gene identification, data visualization, and annotation.

Results

Clinical summary

The six cases were from two females and four males, aged 18–84 (mean 51) years old. The lesions ranged from 0.5 to 5.6 (mean 2.1) cm in the greatest dimensions. Three were located on the back; 3 on the lower extremities (thigh, knee, shin). The clinical impression was highly variable and ranged from benign lesions such as cyst, nevus, or neurofibroma to more concerning diagnoses such as dermatofibrosarcoma protuberans and basal cell carcinoma. Four out of the six cases showed positive margins, and re-excision of the tumor was recommended for three of them. Of the four cases with limited follow-up information (2–18 months; three with positive margins), none recurred. The clinical features are summarized in Table 1.

Histopathologic features

Histopathologically, four cases were confined to the dermis, and two were centered in the subcutis (with limited involvement of the deep dermis). All six cases shared a characteristic growth pattern of ovoid to spindled cells arranged

Table 1 Clinical features.

Case	Age	Sex	Body site	Clinical impression	Greatest dimension (cm)	Tumor at margins	Recommend re-excision	Tumor recurrence	Follow-up (months)
1	74	M	Lower back	Neurofibroma	1.9	Yes	Yes	No	18
2	51	F	Upper back	DFSP	0.5	No	No	N/A	N/A
3	18	M	Lower back	Cyst	2.7	Yes	Yes	N/A	N/A
4	38	F	Right thigh	"Mass"	5.6	Yes	Yes*	No	6
5	43	M	Left knee (proximal pretibial)	Irritated nevus *vs* skin tag	0.9	Yes	Yes	No	4
6	84	M	Right shin	Basal cell carcinoma	0.8	No	No	No	2

DFSP dermatofibrosarcoma protuberans.

*Patient treated with ALK inhibitor but did not undergo re-excision.

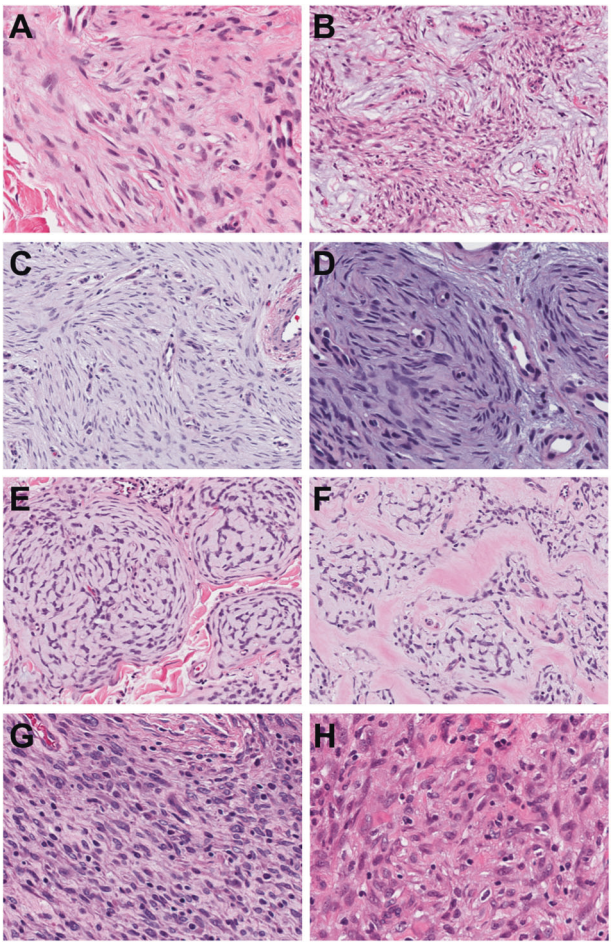

Fig. 1 Myxoid spindled cell whorls and cellular nodules. A Myxoid areas with spindled cells arranged in a swirling pattern (case 2, 400×). **B** Alternating hypocellular myxoid areas with spindled cells arranged in whorls and cellular nodules consisting of plump spindled to ovoid cells (case 3, 200×). **C**, **D** Spindled cells arranged in tight concentric whorls in a myxoid stroma (**C**: case 5, 200×; **D**: case 6, 400×). **E**, **F** Myxohyaline areas with ovoid to spindled cells in cords and chains loosely packed in whorls (**E**: case 1, 200×; **F**: case 4, 400×). **G**, **H** More cellular areas of ovoid to plump spindle cells in loose aggregates. A moderate amount of tumor-infiltrating lymphocytes and plasma cells are present. (**G**: case 4; **H**: case 3; **G**, **H**: 400×). **A**–**H**: H&E.

in perineurial/meningothelial-like concentric whorls and cords in a myxoid to myxohyaline stroma within relatively hypocellular areas. These swirling myxoid nodules ranged from tight concentric whorls (Cases 2, 3, 5, and 6) to less compact nodules (Cases 1 and 4) (Fig. 1A–F). In addition, more cellular areas consisting of aggregates of plump ovoid to epithelioid cells were seen adjacent or admixed with these myxoid spindle cell areas (Fig. 1G, H), imparting a biphasic appearance (Fig. 2A–D). In all but one case, these cells showed no to minimal nuclear atypia, open to fine chromatin, scant to moderate eosinophilic cytoplasm, and indistinct cell borders. The background stroma was variably myxoid to myxohyaline or collagenous. One case (Case 4) exhibited focal nuclear pleomorphism. None of the cases showed conspicuous mitotic activity (<1 mitotic figure per 10 high power fields) or tumor necrosis. Tumor circumscription varied from circumscribed (four cases) to poorly defined (two cases). Four cases showed distinct hyalinized blood vessels (three ectatic, one small, and round), one case had linear to branching, thin-walled vasculature (Case 3), and one had an inconspicuous vasculature (Case 2) (Fig. 2E, F). Three cases had a moderate number of tumor-infiltrating lymphocytes. Two of these cases (Cases 2 and 3) also showed scattered lymphoid aggregates, one of which was most likely related to prior biopsy site changes (Case 2). Two cases showed lipofibromatosis-like areas in the periphery of the tumor (Cases 3 and 4) (Fig. 2G, H). The histopathologic features are summarized in Table 2.

Immunohistochemical features

In all six cases, the tumor cells demonstrated diffuse ALK (D5F3 clone) expression. Interestingly, all but one case also diffusely co-expressed S100 protein and CD34 (one case expressed CD34 but not S100 protein) (Fig. 3A–I). However, the tumor cells in all six cases were negative for EMA, AE1/AE3, SMA, and SOX10 (Table 3).

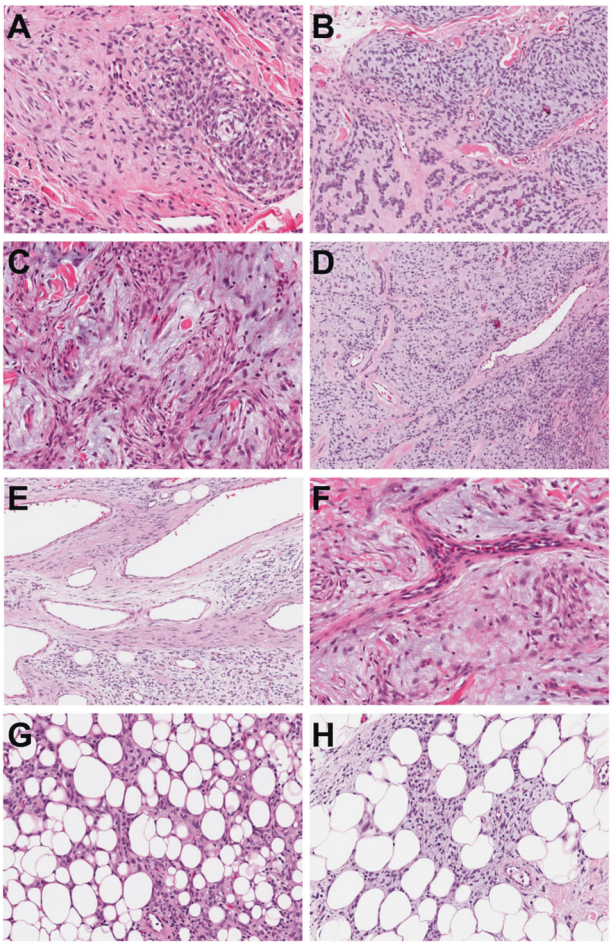

Fig. 2 Biphasic appearance and special histologic features. A–D Low power showing biphasic appearance of alternating hypocellular myxoid spindled cell areas and relatively cellular areas consisting of plump ovoid to epithelioid cells in aggregates and clusters (**A**: case 2, 200×; **B**: case 1, 100×; **C**: case 3, 200×; **D**: case 4, 100×). **E** Ectatic and hyalinized vasculature (case 4, 100×). **F** One case shows numerous linear to branching, thin-walled blood vessels (case 3, 200×). **G**, **H** Lipofibromatosis-like areas in the periphery with spindle cells interdigitating with adipocytes (**G**: case 3; **H**: case 4; **G**, **H**: 200×). **A**–**H**: H&E.

Molecular features

NGS detected *ALK* gene fusions in all six cases. The partner gene of *ALK* was *FLNA* (filamin A) in three cases, *MYH10* (myosin heavy chain 10) in two cases, and *HMBOX1* (homeobox containing 1) in one case (Fig. 4A–D). The *ALK* breakpoint is located at the 5' end of exon 20 of all six cases, which leaves the protein tyrosine kinase domain coding region of ALK intact. Details regarding the protein fusions encoded by the gene fusions are presented in Table 4. There were no specific histopathologic features related to the fusion partner. None of these partners have been previously reported in inflammatory myofibroblastic tumor (IMT) or epithelioid fibrous histiocytoma (EFH),

Table 2 Histologic features.

Case	Extent	Cytomorphology	Growth pattern	Stroma	Border	Tumor vasculature	Inflammation	Atypia	Mitosis (per 10 HPF)
1	Deep dermis	Ovoid to spindled, scant to moderate eosinophilic cytoplasm	Concentric whorls and cords with hyper- and hypocellular zones	Myxo-collagenous	Circumscribed	Small, round, and hyalinized	Absent	Absent	<1
2	Superficial dermis				Poorly circumscribed	Inconspicuous	Moderate, lymphoid aggregates*	Minimal	<1
3	Subcutis				Poorly circumscribed	Linear to branching	Moderate, TILs	Minimal	<1
4	Subcutis				Circumscribed	Ectatic and hyalinized	Moderate, TILs	Moderate	<1
5	Deep dermis				Circumscribed	Ectatic and hyalinized	Minimal	Minimal	<1
6	Deep dermis				Circumscribed	Small, round to ectatic, and hyalinized	Minimal	Minimal	<1

HPF high power fields, *TIL* tumor-infiltrating lymphocytes.
*Previously biopsied.

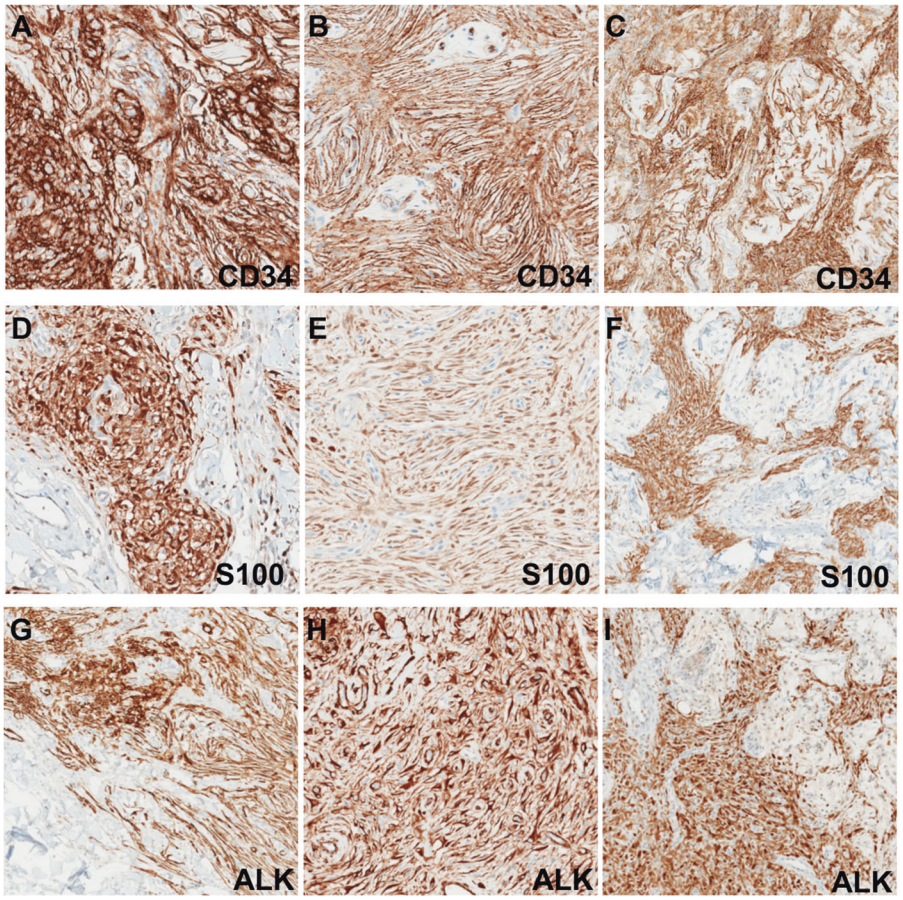

Fig. 3 Immunohistochemical features. Immunohistochemically, the tumor cells exhibit strong and diffuse CD34 (**A**–**C**), S100 (**D**–**F**), and ALK-D5F3 (**G**–**I**) expression. **A**, **D**, **G**: case 2; **B**, **E**, **H**: case 5; **C**, **F**, **I**: case 3.

Table 3 Immunohistochemical features [intensity, extent (%)].

Case	ALK-D5F3	CD34	S100	EMA	AE1/AE3	SMA	SOX10
1	+, diffuse	++, focal	+++, diffuse	−	−	−	−
2	+++, diffuse	+++, diffuse	+++, diffuse	−	−	−	−
3	+++, diffuse	+++, diffuse	+++, diffuse	−	−	−	−
4	+++, diffuse	+++, diffuse	−	−	−	−	−
5	+++, diffuse	+++, diffuse	+++, diffuse	−	−	−	−
6	+++, diffuse	+++, diffuse	+++, diffuse	−	−	−	−

Extent: negative (−): 0%, focal: <50%, diffuse: >50%. Intensity: weak: +, moderate: ++, strong: +++.

both soft tissue tumors characterized by the presence *ALK* gene fusions.

Discussion

To our knowledge, this is the first case series of a novel *ALK*-rearranged cutaneous soft tissue tumor characterized by the presence of myxoid spindle cell whorls and co-expression of CD34 and (usually) S100 protein that we have provisionally termed "Superficial *ALK*-rearranged Myxoid Spindle Cell Neoplasm" (SAMS).

Recently, a large-scale study of 73 soft tissue tumors with a wide spectrum of kinase fusions identified two cases with *ALK* gene fusions [17]. In this study, CD34 was expressed in 89–92% of cases, and S100 was expressed in 64–89% of cases. The two cases that were *ALK*-rearranged were intramuscular and both showed pure lipofibromatosis-like neural tumor histology: one was S100+/CD34−, the other was S100−/CD34+. In addition, a few single case reports of soft tissue and bone tumors with *ALK*-rearrangement and S100 and CD34 coexpression from various anatomic locations have been reported. To our knowledge, these included: a *PP1CB-ALK*-rearranged intramuscular shoulder mass [18], an *EML4-ALK*-rearranged intraosseous vertebral mass [19], and an *EML4-ALK*-rearranged scalp skin lesion with *EML4-ALK* fusion [20]. These *ALK*-rearranged bone and soft tissue tumors are thought to be related

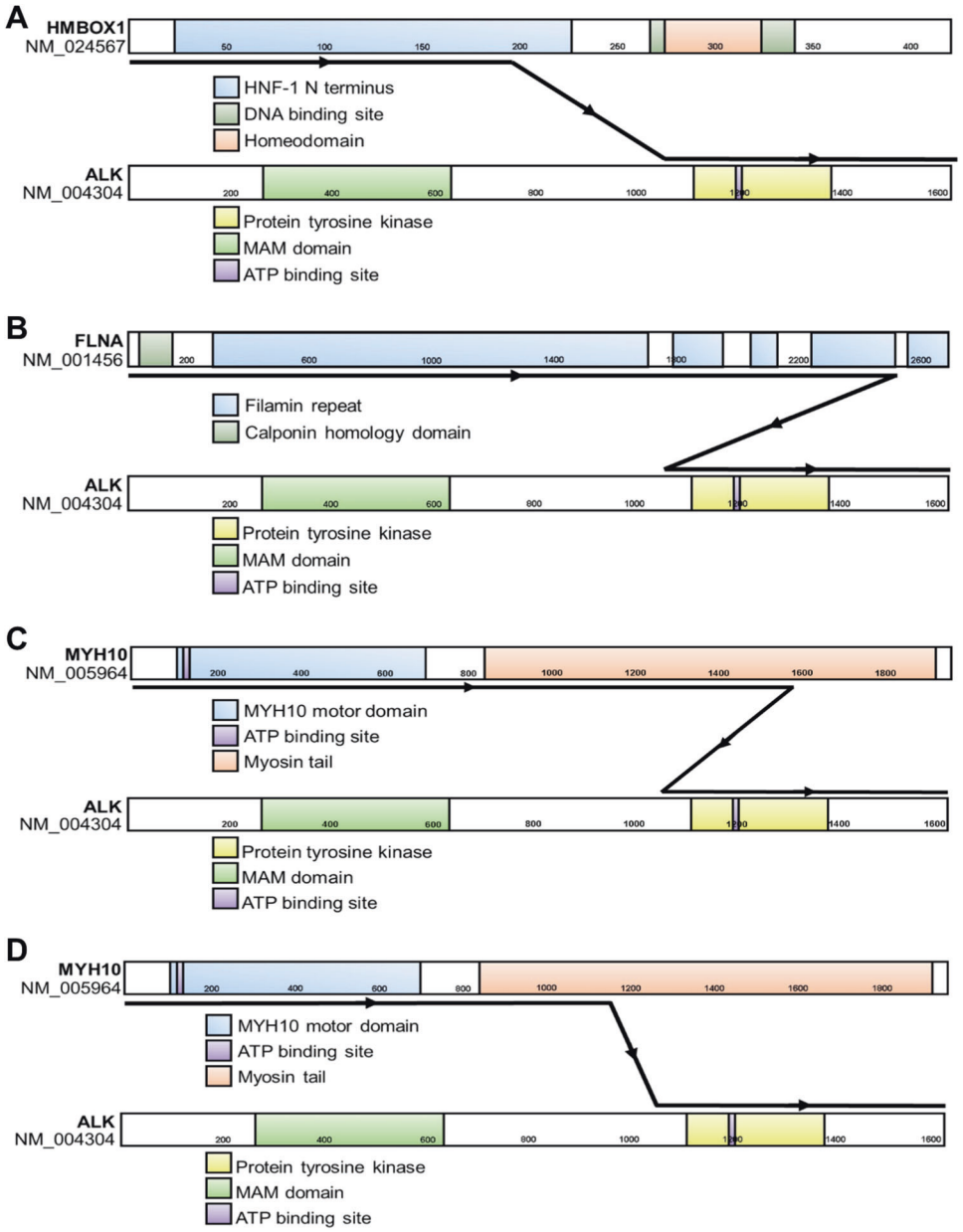

Fig. 4 Schematic of predicted fusion proteins encoded by *ALK* gene fusions. Vertical lines represent the exon boundaries of the encoding genes. Coding amino-acid numbers are denoted. The arrowed line represents the direction of fusion and predicted included domains in the chimeric protein product. **A** *HMBOX1-ALK* [HMBOX1 NM_024567 exon 5 fused to ALK NM_004304 exon 20] (case 1). **B** *FLNA-ALK* [FLNA NM_001456 exon 45 fused to ALK NM_004304 exon 20] (case 2, 5, 6). **C** *MYH10-ALK* [MYH10 NM_005964 exon 33 fused to ALK NM_004304 exon 20] (case 3). **D** *MYH10-ALK* [MYH10 NM_005964 intron 26 fused to ALK NM_004304 exon 20] (case 4). In all six cases, the breakpoints are located in exon 20 of *ALK* and the protein tyrosine kinase domain of ALK is preserved in the fusion product. All figures adapted from ProteinPaint [45].

Table 4 Molecular features.

Case	Fusion	*ALK* partner breakpoint	*ALK* breakpoint	Hg19 chromosomal RNA contig breakpoints (strand direction)
1	*HMBOX1-ALK*	NM_024567 exon 5	NM_004304 exon 20	chr8:28837673(+)::chr2:29446394(−)
2	*FLNA-ALK*	NM_001456 exon 45		chrX:153578017(−)::chr2:29446394(−)
3	*MYH10-ALK*	NM_005964 exon 33		chr17:8393658(−)::chr2:29446503(−)*
4	*MYH10-ALK*	NM_005964 intron 26		chr17:8404483(−)::chr2:29446351
5	*FLNA-ALK*	NM_001456 exon 45		chrX:153578017(−)::chr2:29446394(−)
6	*FLNA-ALK*	NM_001456 exon 45		chrX:153578017(−)::chr2:29446394(−)

*Breakpoint occurs in intron 19 of *ALK*, which still includes exon 20 in the fusion product.

to an emerging class of spindle cell tumors defined by S100 protein and CD34 co-expression and characterized by recurrent tyrosine kinase fusions involving *NTRK1/2/3* [10–13], *BRAF* [10, 14], *RAF1* [10], and *RET* [15, 16]. These tumors exhibit a wide morphologic spectrum and range of clinical behavior. At one end of this spectrum is

lipofibromatosis-like neural tumor, which is a low-grade spindle cell neoplasm showing a highly infiltrative pattern within subcutaneous fat, resembling lipofibromatosis [12].

Given the overall distinctive histopathologic features and different gene rearrangements, it is unclear whether SAMS is related to this emerging class of spindle cell tumors characterized by frequent S100 protein and CD34 co-expression and recurrent tyrosine kinase fusions. It is interesting that the two cases in our series that involve the subcutis exhibit a minor component with lipofibromatosis-like areas, and four cases show perivascular hyalinization, features that have also been reported in prior reports [17, 18, 20]. Nonetheless, the presence of myxoid whorled spindle cell nodules and cords alternating with relatively cellular epithelioid areas in SAMS seems to be a distinctive histologic feature that is relatively unique to this entity. Moreover, all our cases were superficial and dermal-based. And lipofibromatosis-like areas were only a minor component in two of our cases. We have provisionally termed this entity SAMS to reflect the unique histologic features to make it more easily recognizable by pathologists at large. We realize that this could change subsequently if it is determined that SAMS is truly related to the few cases of *ALK*-rearranged tumors with S100 and CD34 coexpression reported thus far.

IMTs are fibroblastic/myofibroblastic tumors characterized by the presence of prominent admixed lymphoplasmacytic inflammation and a wide spectrum of morphologic patterns [22, 23]. Approximately 50–60% of IMTs harbor *ALK* gene fusions [6, 24]. To date, multiple *ALK* gene partners have been reported in IMT: *A2M, ATIC, CARS, CLTC, DCTN1, DES, EML4, FN1, HNRNPA1, IGFBP5, LMNA, PPFIBP1, PRKAR1A, RANBP2, RRBP1, SEC31L1, TFG, THBS1, TIMP3, TNS1, TPM3, TPM4* [6, 23, 25–32], none of which overlap with the *ALK* fusion partners identified in SAMS. In addition, unlike SAMS, IMTs predominantly occur in the deep soft tissue, and cutaneous IMTs are extraordinarily rare [22, 23]. IMTs also exhibit a myofibroblastic phenotype and are thus usually positive for SMA by immunohistochemistry [23]. All cases in this series were negative for SMA.

EFH is a distinct variant of fibrous histiocytoma characterized by the presence of an epidermal collarette. It is a circumscribed dermal-based tumor consisting of plump uniform epithelioid cells, often with peripheral ectatic blood vessels [33, 34]. Of the *ALK* gene partners reported in EFH to date: *DCTN1, EML4, ETV6, MLPH, PPFIBP1, PRKAR2A, SPECC1L, SQSTM1, TMP3, VCL* [7, 8, 35–37], none overlap with the *ALK* fusion partners identified in SAMS. Although EFH also expresses ALK by immunohistochemistry, it is consistently negative for S100 protein, and does not demonstrate the myxoid spindled cell whorls and concentric nodules seen in SAMS [33–35].

Myoepithelial tumors, including myoepitheliomas and myoepithelial carcinomas, often exhibit spindled to epithelioid cells arranged in cords in a myxoid stroma, and variably express S100 protein [38]. However, they also often coexpress epithelial markers (e.g., cytokeratins and EMA) and muscle markers (e.g., SMA), which are consistently negative in all cases of SAMS in our study. In addition, myoepithelial tumors are shown to harbor fusions involving *EWSR1* and occasionally *FUS* [39], but *ALK* rearrangements have never been demonstrated in these tumors.

Perineuriomas are benign peripheral nerve sheath tumors that typically show a predominantly whorled or storiform growth pattern with slender spindle cells exhitibing tapering nuclei and delicate bipolar cytoplasmic processes. Approximately 10% of perineuriomas are limited to the dermis. The stroma in the majority of perineuriomas is collagenous, but ~20% of cases contain focal to abundant myxoid matrix [40]. Although SAMS is also characterized by the presence of spindle cells in a whorled growth pattern, the absence of EMA expression, which is consistently expressed by perineuriomas [40], strongly argues against this diagnosis.

A major weakness of this study is the lack of detailed clinical follow-up information in two of the six patients. Four cases were known to have performed well and did not show local recurrence following excision. For the remaining two cases, the patients were lost to follow-up in the sense that there were no additional encounters in the medical system related to their tumor, which may imply uneventful recovery, although we could not be certain about this. Therefore, the precise long-term clinical behavior of SAMS is uncertain. Based on the histopathologic features, given the lack of significant cytologic atypia and other features including high mitotic rate, atypical mitotic figures, and tumor necrosis, in conjunction with the few cases with no known recurrence post-excision, we suspect that SAMS may exhibit non-aggressive clinical behavior. Should this not prove to be true in subsequent studies, the presence of in-frame *ALK* fusions with preserved protein kinase domains provide a therapeutic target using ALK kinase inhibitors, such as crizotinib, which are already used clinically for the treatment of IMT and *ALK*-mutated non-small cell lung cancers, among others [41].

In terms of oncogenic mechanisms, we hypothesize that the *ALK* gene fusion may lead to constitutive activation of the ALK protein tyrosine kinase (PTK) domain. This may be accomplished by *ALK* partners that allow two ALK PTK domains to interact, leading to dimerization, which is normally required for downstream signaling [2, 3]. For both *FLNA-ALK* and *MYH10-ALK* fusions, since the breakpoints occur near the C-terminals of the FLNA and MYH10 proteins, the majority of their protein domains (encompassing the filamin repeats and MYH10 motor domains,

respectively) are preserved and attached to the tyrosine kinase domain of ALK. Both FLNA and MYH10 are involved in cytoskeleton remodeling/reorganization and have a broad expression in human tissues [42, 43]. It is possible that, since these proteins interact with actin and the cytoskeleton, the fusion proteins may also localize to the same subcellular location, thus bringing two PTK domains together for dimerization. On the other hand, *HMBOX1* has ubiquitous expression and is involved with telomere elongation. It has a homeodomain that binds directly to telomeric DNA. HMBOX1 is predominantly found in the cytoplasm, however, it also localizes to the nucleus where it binds to active telomeres [44]. In the case of *HMBOX1-ALK* fusion, the breakpoint occurs earlier in the gene, near the end of the HNF-1 N domain. As such, the homeodomain is lost. We speculate that with this loss of telomeric-binding capacity, the HMBOX1-ALK chimeric protein likely remains in the cytoplasm, similar to FLNA and MYH10 chimeric products.

In conclusion, we report the first case series of a novel *ALK*-rearranged cutaneous soft tissue tumor characterized by the presence of myxoid spindle cell whorls and cords, and expression of ALK, CD34, and frequently S100 protein. This entity, termed "Superficial ALK-rearranged Myxoid Spindle Cell Neoplasm" (SAMS), exhibits unique morphologic, immunophenotypic, and genetic features that are not shared by other entities with *ALK* fusions. Future studies are needed to better characterize the full spectrum of histopathologic findings and long-term clinical behavior of SAMS.

Data availability

Data sharing is not applicable to this article as no data sets were generated or analyzed during the current study.

Author contributions J.K.D. performed study design, acquisition, analysis, and interpretation of data, writing, and revision of the paper. E.M.A. performed analysis and interpretation of data and writing of the paper. J.R.G. and B.P.R. performed review of the paper and interpretation of data. S.D.B. and J.S.K. performed study design and conception, analysis and interpretation of data, review, and revision of the paper. All authors read and approved the final manuscript.

Funding All authors report no funding sources related to this study.

Compliance with ethical standards

Ethics approval/consent to participate This study was approved by the Cleveland Clinic Institutional Review Board (#06-977).

Conflict of interest The authors declare no competing interests.

Publisher's note Springer Nature remains neutral with regard to jurisdictional claims in published maps and institutional affiliations.

References

1. Shiota M, Fujimoto J, Semba T, Satoh H, Yamamoto T, Mori S. Hyperphosphorylation of a novel 80 kDa protein-tyrosine kinase similar to Ltk in a human Ki-1 lymphoma cell line, AMS3. Oncogene. 1994;9:1567–74.
2. Hallberg B, Palmer RH. The role of the ALK receptor in cancer biology. Ann Oncol 2016;27:iii4–15.
3. Hallberg B, Palmer RH. Mechanistic insight into ALK receptor tyrosine kinase in human cancer biology. Nat Rev Cancer. 2013; 13:685–700.
4. Soda M, Choi YL, Enomoto M, Takada S, Yamashita Y, Ishikawa S, et al. Identification of the transforming EML4-ALK fusion gene in non-small-cell lung cancer. Nature. 2007;448:561–6.
5. Morris SW, Kirstein MN, Valentine MB, Dittmer KG, Shapiro DN, Saltman DL, et al. Fusion of a kinase gene, ALK, to a nucleolar protein gene, NPM, in non-Hodgkin's lymphoma. Science. 1994;263:1281–4.
6. Bridge JA, Kanamori M, Ma Z, Pickering D, Hill DA, Lydiatt W, et al. Fusion of the ALK gene to the clathrin heavy chain gene, CLTC, in inflammatory myofibroblastic tumor. Am J Pathol 2001; 159:411–5.
7. Doyle LA, Mariño-Enriquez A, Fletcher CD, Hornick JL. ALK rearrangement and overexpression in epithelioid fibrous histiocytoma. Mod Pathol 2015;28:904–12.
8. Dickson BC, Swanson D, Charames GS, Fletcher CD, Hornick JL. Epithelioid fibrous histiocytoma: molecular characterization of ALK fusion partners in 23 cases. Mod Pathol 2018;31:753–62.
9. Amin SM, Haugh AM, Lee CY, Zhang B, Bubley JA, Merkel EA, et al. A comparison of morphologic and molecular features of BRAF, ALK, and NTRK1 fusion spitzoid neoplasms. Am J Surg Pathol 2017;41:491–8.
10. Suurmeijer AJH, Dickson BC, Swanson D, Zhang L, Sung YS, Cotzia P, et al. A novel group of spindle cell tumors defined by S100 and CD34 co-expression shows recurrent fusions involving RAF1, BRAF, and NTRK1/2 genes. Genes Chromosomes Cancer. 2018;57:611–21.
11. Davis JL, Lockwood CM, Stohr B, Boecking C, Al-Ibraheemi A, DuBois SG, et al. Expanding the spectrum of pediatric NTRK-rearranged mesenchymal tumors. Am J Surg Pathol 2019;43: 435–45.
12. Agaram NP, Zhang L, Sung YS, Chen CL, Chung CT, Antonescu CR, et al. Recurrent NTRK1 gene fusions define a novel subset of locally aggressive lipofibromatosis-like neural tumors. Am J Surg Pathol 2016;40:1407–16.
13. Suurmeijer AJ, Dickson BC, Swanson D, Zhang L, Sung YS, Huang HY, et al. The histologic spectrum of soft tissue spindle cell tumors with NTRK3 gene rearrangements. Genes Chromosomes Cancer. 2019;58:739–46.
14. Kao YC, Fletcher CDM, Alaggio R, Wexler L, Zhang L, Sung YS, et al. Recurrent BRAF gene fusions in a subset of pediatric spindle cell sarcomas: expanding the genetic spectrum of tumors with overlapping features with infantile fibrosarcoma. Am J Surg Pathol 2018;42:28–38.
15. Davis JL, Vargas SO, Rudzinski ER, López Marti JM, Janeway K, Forrest S, et al. Recurrent RET gene fusions in paediatric spindle mesenchymal neoplasms. Histopathology. 2020;76:1032–41.
16. Antonescu CR, Dickson BC, Swanson D, Zhang L, Sung YS, Kao YC, et al. Spindle cell tumors with RET gene fusions exhibit a morphologic spectrum akin to tumors with NTRK gene fusions. Am J Surg Pathol 2019;43:1384–91.
17. Kao YC, Suurmeijer AJH, Argani P, Dickson BC, Zhang L, Sung YS, et al. Soft tissue tumors characterized by a wide spectrum of kinase fusions share a lipofibromatosis-like neural tumor pattern. Genes Chromosomes Cancer. 2020;59:575–83.

18. Lopez-Nunez O, Surrey LF, Alaggio R, Fritchie KJ, John I. Novel PPP1CB-ALK fusion in spindle cell tumor defined by S100 and CD34 coexpression and distinctive stromal and perivascular hyalinization. Genes Chromosomes Cancer. 2020;59:495–9.
19. Mantilla JG, Cheung H, Ha AS, Hoch BL, Liu YJ, Ricciotti RW. Spindle cell neoplasm with EML4-ALK gene fusion presenting as an intraosseous vertebral mass. Genes Chromosomes Cancer. 2021;60:282–6.
20. Abs D, Landman S, Osio A, Lepesant P, Schneider P, Obadia D, et al. Spindle cell tumor with CD34 and S100 co-expression and distinctive stromal and perivascular hyalinization showing EML4-ALK fusion. J. Cutan. Pathol. https://doi.org/10.1111/cup.13926 (2020).
21. Cheng YW, Meyer A, Jakubowski MA, Keenan SO, Brock JE, Azzato EM, et al. Gene fusion identification using anchor-based multiplex PCR and next-generation sequencing. J. Appl. Lab. Med. https://doi.org/10.1093/jalm/jfaa230 (2021).
22. Coffin CM, Hornick JL, Fletcher CD. Inflammatory myofibroblastic tumor: comparison of clinicopathologic, histologic, and immunohistochemical features including ALK expression in atypical and aggressive cases. Am J Surg Pathol 2007;31:509–20.
23. Bennett JA, Nardi V, Rouzbahman M, Morales-Oyarvide V, Nielsen GP, Oliva E. Inflammatory myofibroblastic tumor of the uterus: a clinicopathological, immunohistochemical, and molecular analysis of 13 cases highlighting their broad morphologic spectrum. Mod Pathol 2017;30:1489–503.
24. Griffin CA, Hawkins AL, Dvorak C, Henkle C, Ellingham T, Perlman EJ. Recurrent involvement of 2p23 in inflammatory myofibroblastic tumors. Cancer Res 1999;59:2776–80.
25. Haimes JD, Stewart CJR, Kudlow BA, Culver BP, Meng B, Koay E, et al. Uterine Inflammatory myofibroblastic tumors frequently harbor ALK fusions with IGFBP5 and THBS1. Am J Surg Pathol 2017;41:773–80.
26. Inamura K, Kobayashi M, Nagano H, Sugiura Y, Ogawa M, Masuda H, et al. A novel fusion of HNRNPA1-ALK in inflammatory myofibroblastic tumor of urinary bladder. Hum Pathol 2017;69:96–100.
27. Lovly CM, Gupta A, Lipson D, Otto G, Brennan T, Chung CT, et al. Inflammatory myofibroblastic tumors harbor multiple potentially actionable kinase fusions. Cancer Discov 2014;4:889–95.
28. Tanaka M, Kohashi K, Kushitani K, Yoshida M, Kurihara S, Kawashima M, et al. Inflammatory myofibroblastic tumors of the lung carrying a chimeric A2M-ALK gene: report of 2 infantile cases and review of the differential diagnosis of infantile pulmonary lesions. Hum Pathol 2017;66:177–82.
29. Debelenko LV, Arthur DC, Pack SD, Helman LJ, Schrump DS, Tsokos M. Identification of CARS-ALK fusion in primary and metastatic lesions of an inflammatory myofibroblastic tumor. Lab Invest 2003;83:1255–65.
30. Mariño-Enríquez A, Wang WL, Roy A, Lopez-Terrada D, Lazar AJ, Fletcher CD, et al. Epithelioid inflammatory myofibroblastic sarcoma: An aggressive intra-abdominal variant of inflammatory myofibroblastic tumor with nuclear membrane or perinuclear ALK. Am J Surg Pathol 2011;35:135–44.
31. Chen ST, Lee JC. An inflammatory myofibroblastic tumor in liver with ALK and RANBP2 gene rearrangement: combination of distinct morphologic, immunohistochemical, and genetic features. Hum Pathol 2008;39:1854–8.
32. Takeuchi K, Soda M, Togashi Y, Sugawara E, Hatano S, Asaka R, et al. Pulmonary inflammatory myofibroblastic tumor expressing a novel fusion, PPFIBP1-ALK: reappraisal of anti-ALK immunohistochemistry as a tool for novel ALK fusion identification. Clin Cancer Res 2011;17:3341–8.
33. Singh Gomez C, Calonje E, Fletcher CD. Epithelioid benign fibrous histiocytoma of skin: clinico-pathological analysis of 20 cases of a poorly known variant. Histopathology. 1994;24:123–9.
34. Glusac EJ, Barr RJ, Everett MA, Pitha J, Santa Cruz DJ. Epithelioid cell histiocytoma. A report of 10 cases including a new cellular variant. Am J Surg Pathol 1994;18:583–90.
35. Kazakov DV, Kyrpychova L, Martinek P, Grossmann P, Steiner P, Vanecek T, et al. ALK gene fusions in epithelioid fibrous histiocytoma: a study of 14 cases, with new histopathological findings. Am J Dermatopathol 2018;40:805–14.
36. Nakayama R, Togashi Y, Baba S, Kaku Y, Teramoto Y, Sakurai T, et al. Epithelioid cell histiocytoma with SQSTM1-ALK fusion: a case report. Diagn Pathol 2018;13:28.
37. Jedrych J, Nikiforova M, Kennedy TF, Ho J. Epithelioid cell histiocytoma of the skin with clonal ALK gene rearrangement resulting in VCL-ALK and SQSTM1-ALK gene fusions. Br J Dermatol 2015;172:1427–9.
38. Hornick JL, Fletcher CD. Myoepithelial tumors of soft tissue: a clinicopathologic and immunohistochemical study of 101 cases with evaluation of prognostic parameters. Am J Surg Pathol 2003;27:1183–96.
39. Antonescu CR, Zhang L, Chang NE, Pawel BR, Travis W, Katabi N, et al. EWSR1-POU5F1 fusion in soft tissue myoepithelial tumors. A molecular analysis of sixty-six cases, including soft tissue, bone, and visceral lesions, showing common involvement of the EWSR1 gene. Genes Chromosomes Cancer. 2010;49:1114–24.
40. Hornick JL, Fletcher CD. Soft tissue perineurioma: clinicopathologic analysis of 81 cases including those with atypical histologic features. Am J Surg Pathol 2005;29:845–58.
41. Mossé YP, Lim MS, Voss SD, Wilner K, Ruffner K, Laliberte J, et al. Safety and activity of crizotinib for paediatric patients with refractory solid tumours or anaplastic large-cell lymphoma: a Children's Oncology Group phase 1 consortium study. Lancet Oncol 2013;14:472–80.
42. Nakamura F, Stossel TP, Hartwig JH. The filamins: organizers of cell structure and function. Cell Adh Migr 2001;5:160–9.
43. Vicente-Manzanares M, Ma X, Adelstein RS, Horwitz AR. Non-muscle myosin II takes centre stage in cell adhesion and migration. Nat Rev Mol Cell Biol 2009;10:778–90.
44. Kappei D, Butter F, Benda C, Scheibe M, Draskovic I, Stevense M, et al. HOT1 is a mammalian direct telomere repeat-binding protein contributing to telomerase recruitment. EMBO J 2013;32:1681–701.
45. Zhou X, Edmonson MN, Wilkinson MR, Patel A, Wu G, Liu Y, et al. Exploring genomic alteration in pediatric cancer using ProteinPaint. Nat Genet 2016;48:4–6.